American Mineralogist, Volume 68, pages 1189–1198, 1983

The crystal structure of $CaGeO_3$ perovskite and the crystal chemistry of the $GdFeO_3$-type perovskites

SATOSHI SASAKI, CHARLES T. PREWITT AND ROBERT C. LIEBERMANN

Department of Earth and Space Sciences
State University of New York, Stony Brook, New York 11794

Abstract

A single-crystal X-ray study indicates that the perovskite form of $CaGeO_3$ is orthorhombic (*Pbnm*), and isotypic with $GdFeO_3$, although it was previously reported as a cubic form; the cell dimensions are $a = 5.2607(6)$Å, $b = 5.2688(10)$, $c = 7.4452(15)$ and $V = 206.36(6)$Å^3 ($Z = 4$; $D_{calc} = 5.17$ g/cm^3). The crystal structure is close to that of $SmAlO_3$. Although the unit cell of $CaGeO_3$ is pseudocubic, the structure itself is very distorted through the tilting and distortion of polyhedra. The oxygen polyhedra are less tilted and less distorted than those of other $GdFeO_3$-type perovskites. The structural deformation of the $GdFeO_3$-type perovskite is determined primarily by the size-ratio of two kinds of cation occupying A and B sites. Some structural characteristics such as O(2)–O(2)–O(2) and A–O(1)–B angles and bond-length distortions exhibit systematic relationships as a function of the observed tolerance factor which is newly defined here. A strong correlation between the Goldschmidt tolerance factor and the observed tolerance factor has made possible some predictions for $GdFeO_3$-type perovskites.

Introduction

The perovskite structure, with general formula ABO_3, consists of a framework of B octahedra that share corners with each other and triangular faces with cuboctahedra containing A cations in twelve coordination. For compositions in which their constituent atoms are not of the ideal relative size, many distorted types of perovskite may replace the ideal structure. Some metasilicates and metagermanates are known to crystallize as perovskites in cubic ($SrGeO_3$; above 50 kbar), hexagonal ($BaGeO_3$; above 95 kbar), and orthorhombic phases ($MgSiO_3$; above 300 kbar) (Shimizu *et al.*, 1970; Liu, 1976a; Yagi *et al.*, 1978; Ito and Matsui, 1978). The high-pressure transformation of a metasilicate to a perovskite form is geophysically important for interpreting seismic wave velocities in the Earth's lower mantle. Also, germanates are useful as structural analogs of common silicate minerals at high pressures because new dense phases frequently exist at much lower pressures than the corresponding isotypic silicates.

$CaGeO_3$ is a typical example of such germanates and is known to transform from the wollastonite through a garnet-like structure to the perovskite structure at more than 65 kbar and 900°C (Susaki and Akimoto, private comm.). $CaGeO_3$ has previously been indexed as cubic perovskite with $a = 3.723$Å (Ringwood and Major, 1967), although Prewitt and Sleight (1969) reported a doubling of the unit cell ($a = 7.448$Å). In order to confirm the cell dimension and the space group of $CaGeO_3$ perovskite, we examined a single crystal using X-ray diffraction techniques, to refine its crystal structure, and to make a systematic study of crystallographic correlations among the $GdFeO_3$-type perovskites. A preliminary communication on this result has been reported (Sasaki *et al.*, 1981).

Experimental

Sample

A polycrystalline specimen of $CaGeO_3$ perovskite was synthesized by hot-pressing $CaGeO_3$ wollastonite powder in squeezer solid-media apparatus for two hours at $P = 100$ kbar and at $T = 1000$°C (see details in Liebermann *et al.*, 1977). After sintering at elevated pressure and temperature, the run was slowly cooled (20–60 minutes) to room temperature after which the pressure was released. Examination of the recovered specimen using a polarizing microscope and X-ray powder diffraction analyses confirmed that it was a single phase with the perovskite structure. A single crystal of parallelepiped shape and dimensions, $0.14 \times 0.10 \times 0.07$ mm was extracted from the polycrystalline aggregate and prepared for single-crystal X-ray diffraction study.

Space group determination

The unit cell and space group of $CaGeO_3$ perovskite were determined with the aid of precession and Weissenberg photographs and intensity data collected with a Picker four-circle diffractometer. The space group deter-

0003–004X/83/1112–1189$02.00

mination was more difficult than expected, because the unit cell is pseudocubic, dimensionally and in intensity distribution for strong reflections. The cell dimensions determined with the four-circle diffractometer (graphite monochromatized Mo$K\alpha_1$; λ = 0.70926Å) are as follows:

a = 5.2607(6)Å
b = 5.2688(10)
c = 7.4452(15)
V = 206.36(6)Å^3
Z = 4 (formula units/cell)
D_{calc} = 5.17 g/cm^3

The cell dimensions have the relation $a \cong b \cong \sqrt{2}\, a_p$ and $c \cong 2a_p$ (a_p: a pseudocubic subcell parameter), maintaining the characteristic of $GdFeO_3$-type perovskites. In order to emphasize the difference from cubic perovskite, the precession photograph for $hk1$ is shown in Figure 1. If this crystal were cubic with a = 3.7Å, no diffraction spots would appear on photographs for $l = 2n + 1$ on the orthorhombic cell. The intensity distribution indicates orthorhombic symmetry. The systematic absences are: no conditions on hkl; $k = 2n$ on $0kl$; $h + l = 2n$ on $h0l$; no conditions on $hk0$; ($h = 2n$) on $h00$; ($k = 2n$) on $0k0$; ($l = 2n$) on $00l$. The possible space group is either D_{2h}^{16}-*Pbnm* or C_{2v}^{9}-*Pbn*2_1. On the basis of no evidence for noncentrosymmetry and the results of least-squares refinement of the structure, the space group is most likely *Pbnm*. Although some weak reflections apparently violating the above determination could be detected, they were reflections caused by a small twinned part of the crystal, as will be described in the following section.

Twinning

Preliminary investigation using the four-circle diffractometer and long-exposure precession photographs showed the presence of two types of reflections inconsistent with the $GdFeO_3$-type perovskite of space group *Pbnm*. The first type is of reflections on the reciprocal points at half-integral coordinates, such as 1/2 5/2 0, 1/2 5/2 2, 1/2 3/2 3, 1/2 1/2 4, 1/2 5/2 4, 3/2 3/2 6, and 1/2 5/2 6. Another is of the 031 and 013 reflections that apparently violate the extinction rule for the b-glide plane. All of the above reflections, however, can be clearly explained by the existence of twinning related by the following transformation matrices:

$$\begin{pmatrix} a^{*\prime} \\ b^{*\prime} \\ c^{*\prime} \end{pmatrix} = \begin{pmatrix} 1/2 & -1/2 & 1 \\ 1/2 & -1/2 & -1 \\ 1/2 & 1/2 & 0 \end{pmatrix} \begin{pmatrix} a^* \\ b^* \\ c^* \end{pmatrix}$$

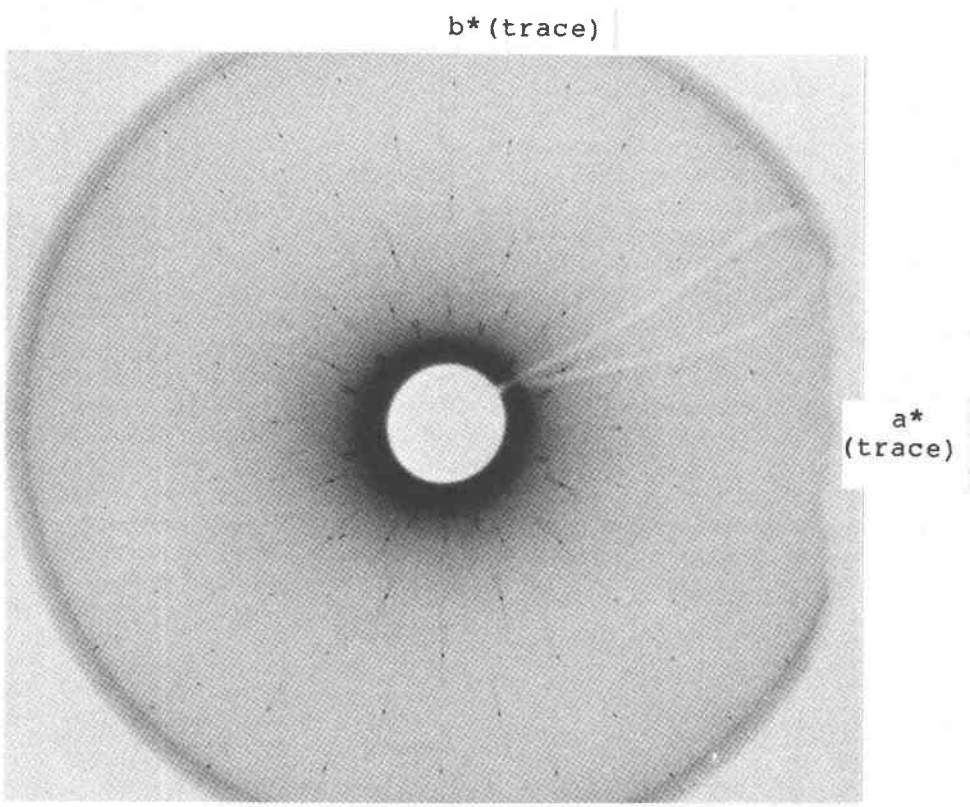

Fig. 1. Precession photograph of the $hk1$ net for $CaGeO_3$ perovskite, taken with μ = 25° (non-filtered Mo$K\alpha$ radiation; 35 kV and 15 mA for 336 hours). If this perovskite were cubic with a = 3.7Å, no diffraction spots would appear for this net. The symmetry *mmm* (orthorhombic) is required for Laue group.

Table 1. Fractional atomic coordinates and thermal parameters ($\times 10^4$) of $CaGeO_3$ perovskite obtained in least-squares refinements: (1) after and (2) before the correction of intensities diffracted by the twinned crystal. The β_{ij}'s are defined by $\exp\{-(h^2\beta_{11}+k^2\beta_{22}+l^2\beta_{33}+2hk\beta_{12}+2hl\beta_{13}+2kl\beta_{23})\}$.

	Ca	Ge	O(1)	O(2)
(1) After correction:				
x	-.0051(3)	0	0.0606(9)	0.7157(6)
y	0.0283(2)	1/2	0.4916(8)	0.2830(6)
z	1/4	0	1/4	0.0320(5)
β11	46(2)	21(1)	36(7)	49(5)
β22	66(2)	25(1)	66(8)	48(5)
β33	30(1)	10(1)	15(4)	24(2)
β12	-9(2)	0(1)	4(6)	-16(5)
β13	0	-0(1)	0	1(3)
β23	0	-0(.4)	0	17(3)
B(equiv)	0.64(2)	0.24(1)	0.49(8)	0.53(5)
Ref.(meas)	689			
(used)	412			
R	0.035			
R(wt)	0.037			
(2) Before correction:				
x	-.0051(5)	0	0.0587(16)	0.7159(10)
y	0.0273(3)	1/2	0.4911(17)	0.2829(9)
z	1/4	0	1/4	0.0321(9)
β11	46(4)	24(3)	42(17)	56(13)
β22	68(4)	31(3)	118(23)	49(12)
β33	24(4)	11(3)	22(17)	34(11)
β12	-6(7)	-0(3)	2(17)	-20(11)
β13	0	0(2)	0	11(10)
β23	0	0(1)	0	1(10)
B(equiv)	0.60(6)	0.29(4)	0.75(27)	0.64(17)
Ref.(meas)	689			
(used)	343*			
R	0.035			
R(wt)	0.052			

*The reflections greater than 4σ were used in refinement.

$$\begin{pmatrix} h' \\ k' \\ l' \end{pmatrix} = \begin{pmatrix} 1/2 & -1/2 & 1/2 \\ 1/2 & -1/2 & -1/2 \\ 1 & 1 & 0 \end{pmatrix} \begin{pmatrix} h \\ k \\ l \end{pmatrix}$$

There is no doubling of spots or peaks for any reflections that overlap. Since the reflections at half integral reciprocal points do not overlap each other, the comparison in intensities of such reflections gave roughly the volume ratio of 1:0.14(1).

Data collection and structure refinement

The ω-2θ scan technique of the four-circle diffractometer was used to collect at room temperature the intensity data up to $2\theta = 80°$ in the bisecting mode. Each reflection was scanned at the appropriate speed with a maximum measurement time of four minutes; the scan width on 2θ (°) was $2.0 + 0.7 \tan\theta$. A standard reflection used was stable within ±1.5% of the integrated intensity during data collection. Of a total of 689 reflections measured, the reflections less than three times the calculated standard deviation were omitted in refinements. A set of intensities was corrected for Lorentz and polarization factors and a prismatic absorption correction was applied using the program ACACA (Wuensch and Prewitt, 1965). The linear absorption coefficient is 177.1 cm^{-1} and the transmission factors for this crystal varied from 0.19 to 0.33.

All parameters were refined simultaneously using the full-matrix least-squares program, RADY, which is a modified version of RADIEL (Coppens *et al.*, 1979). The

Table 2. Interatomic distances (Å) and angles (°) in the Ge octahedron. Standard deviations are in parentheses. Square brackets, [ ], show the value calculated for the ideal cubic perovskite with the same polyhedral volumes.

Ge i - O(1) i x 2		1.889(.9)
- O(2) v x 2		1.898(3)
- O(2) viii x 2		1.889(3)
Mean <Ge - O>		1.892 [1.861]
Bond-length distortion, Δ_B		0.005
O(1) i - O(2) v x 2		2.684(5)
- O(2) iv x 2		2.665(5)
- O(2) i x 2		2.671(5)
- O(2) viii x 2		2.677(5)
O(2) v - O(2) viii x 2		2.659(4)
- O(2) iv x 2		2.696(4)
Mean <O - O>		2.675 [2.632]
O(1) i - Ge i - O(2) viii		90.3(2)
O(1) i - - O(2) v		90.3(2)
O(2) v - - O(2) viii		89.2(1)
O(2) i - - O(2) viii		90.8(1)

Table 3. Interatomic distances (Å) and angles (°) with standard deviation in parentheses for cuboctahedron. Square bracket, [ ], shows the value calculated for the ideal cubic perovskite with the same polyhedral volume.

Ca i - O(1) i x 1			2.346(5)
- O(1) iv x 1			2.465(5)
- O(1) iii x 1			2.929(5)
- O(1) v x 1			2.849(5)
- O(2) i′ x 2			2.352(4)
- O(2) iv′ x 2			2.568(4)
- O(2) v x 2			2.597(4)
- O(2) viii x 2			3.069(4)
Mean <M - O>			2.647 [2.632]
Bond-length distortion, Δ			9.40
O(1) i - O(1) v x 2			3.303(7)
O(1) v - O(1) iii x 2			4.197(7)
- O(2) vii x 4			2.684(5)
- O(2) ii′ x 4			2.665(5)
O(1) iv - O(2) iii′ x 4			2.671(5)
- O(2) vi x 4			2.677(5)
O(2) i′ - O(2) ii′ x 2			3.246(5)
O(2) vii - O(2) viii x 2			4.199(6)
O(2) i′ - O(2) iv′ x 4			2.659(4)
O(2) iii′ - O(2) vi x 4			2.696(4)
O(2) i′ - O(2) iii′ x 4			4.196(5)
- O(2) vii x 4			4.571(5)
- O(2) v x 2			3.256(4)
O(2) iv′ - O(2) viii x 2			4.251(4)
O(1) i - Ca i - O(1) iv		x 1	86.67(16)
O(1) iv - - O(1) iii		x 1	101.83(15)
O(1) iii - - O(1) v		x 1	93.18(13)
O(1) v - - O(1) i		x 1	78.31(15)
O(2) v - - O(2) vi		x 2	107.89(11)
O(2) iii′ - - O(2) iv′		x 2	78.41(12)
O(2) i′ - - O(2) v		x 2	82.13(11)
O(2) iv′ - - O(2) viii		x 2	97.51(10)
O(2) vii - - O(2) viii		x 2	86.34(10)
O(2) i′ - - O(2) ii′		x 2	87.27(13)
O(2) v - - O(2) viii		x 2	55.23(9)
O(2) viii - - O(2) i′		x 2	57.85(10)
O(2) i′ - - O(2) iv′		x 2	65.26(11)
O(2) iv′ - - O(2) v		x 2	62.92(10)
O(1) i - - O(2) vii		x 2	57.42(9)
O(1) v - - O(2) vii		x 2	53.79(8)
O(1) v - - O(2) ii′		x 2	60.77(10)
O(1) iii - - O(2) ii′		x 2	59.58(10)
O(1) iii - - O(2) iii′		x 2	57.56(10)
O(1) iv - - O(2) iii′		x 2	64.06(11)
O(1) iv - - O(2) vi		x 2	63.80(9)
O(1) i - - O(2) vi		x 2	65.54(9)

Table 4. The metal-metal distances (Å) and Ge–O–Ge and O(2)–O(2)–O(2) angles (°), with standard deviations in parentheses.

Ge i - Ge iii	3.7227(4)
- Ge ii	3.7226(8)
Ca i - Ca iii	3.7606(19)
- Ca v	3.6853(19)
- Ca ii	3.7349(8)
Ca i - Ge i	3.248(1)
- Ge iii	3.349(1)
- Ge v	3.204(1)
- Ge vii	3.105(1)
Ge i - O(1) i - Ge ii	160.4(3)
- O(2) viii - Ge iii	159.0(2)
Ca i - O(1) i - Ge i	99.6(1)
Ca iii - O(1) i - Ge i	90.0(1)
Ca i - O(2) i' - Ge v	97.3(1)
- O(2) iv' - Ge v	90.6(1)
- O(2) iv' - Ge vii	86.7(1)
- O(2) v - Ge vii	86.1(1)
- O(2) v - Ge i	91.2(1)
- O(2) viii - Ge i	77.9(1)
- O(2) viii - Ge iii	81.1(1)
- O(2) i' - Ge iii	103.8(1)
O(2) i - O(2) viii - O(2) i'	154.72(18)
O(2) viii- O(2) i' - O(2) iv'	105.10(14)
O(2) i' - O(2) ii' - O(2) vii	100.18(14)

residuals of the function $\Sigma w_i(|F_{obs}|-|F_{calc}|)_i^2$ were minimized with w_i kept as unity. Atomic scattering factor tables and anomalous dispersion coefficients were taken from *International Tables for X-Ray Crystallography, Vol. IV* (1974), Fukamachi (1971), and Tokonami (1964) and a secondary extinction correction was applied following Becker and Coppens (1974).

Results and discussion

Crystal structure of $CaGeO_3$

The final positional and thermal parameters obtained are listed in Table 1[1], in which we include data both before and after correction for the intensity of the twinned crystal. As seen from the table, the shift of atomic parameters due to the twinned crystal is relatively small. The interatomic distances and angles are also given in Tables 2, 3, and 4. Figure 2 shows a projection of the $CaGeO_3$ structure on (001) along with labels for the atoms related by symmetry operations. The atomic coordinates for this perovskite structure are similar to those of $SmAlO_3$ (Marezio *et al.*, 1972).

The cell distortion factor, d, is useful for estimating the departure from an ideal cubic model (for which $d = 0$):

$$d = \{(a/\sqrt{2} - a_p)^2 + (b/\sqrt{2} - a_p)^2 + (c/2 - a_p)^2\}/3a_p^2 \times 10^4,$$

where ($a_p = (a/\sqrt{2} + b/\sqrt{2} + c/2)/3$. The value for $CaGeO_3$ ($d = 0.004$) is close to that for $SmAlO_3$ (0.003) and is much smaller than those for $ScAlO_3$ (5.64), $GdTiO_3$ (6.00), and $GdFeO_3$ (4.08). Although the cell for $CaGeO_3$ is dimensionally close to being cubic, the polyhedra are considerably distorted as in characteristic orthorhombic perovskites. The most prominent distortion from the ideal cubic perovskite is in the tilting of the polyhedra (Fig. 2). The $O(2)^{i}$–$O(2)^{viii}$–$O(2)^{i'}$ angle, which shows the degree of the tilting in the *xy* plane, is 154.7(2)° in contrast to 180° for a cubic perovskite. The value of $O(2)^{i'}$–$O(2)^{ii'}$–$O(2)^{vii}$ angle, corresponding to the tilting on the *xz* plane, is 100.2(1)° as opposed to 90° for a cubic perovskite. The polyhedra themselves have the following characteristics: (1) The ratio of $(\langle M\text{–}O\rangle - \langle M\text{–}O\rangle_{cubic})/\langle M\text{–}O\rangle$ shows that the oxygens around the Ge atom are more extended from the ideal cubic positions (0.016) than those around Ca (0.006), where $\langle M\text{–}O\rangle_{cubic}$ was estimated by constraining a cubic cell to have the same volume as the actual unit cell (see Table 2). (2) When we define the bond-length distortion, Δ, as $1/n\ \Sigma\{(r_i - r)/r\}^2 \times 10^3$, it is clear that the Ca cuboctahedron ($\Delta_A = 9.4$) is distorted, whereas the Ge octahedron is close to a regular one ($\Delta_B = 0.005$). The $SmAlO_3$ perovskite has similar values of the bond-length distortion: $\Delta_A = 8.7$ and $\Delta_B = 0.001$. The distortions, however, are less than for those of most $GdFeO_3$-type perovskites such as $MgSiO_3$ ($\Delta_A = 27.31$, $\Delta_B = 0.226$), $ScAlO_3$ ($\Delta_A = 37.50$, $\Delta_B = 0.034$) and $GdFeO_3$ ($\Delta_A = 28.13$, $\Delta_B = 0.032$). (3) The O–Ca–O angles, which in the ideal cubic perovskite are all 90°, vary from 107.9(1)° to 53.79(8)° (see Table 3).

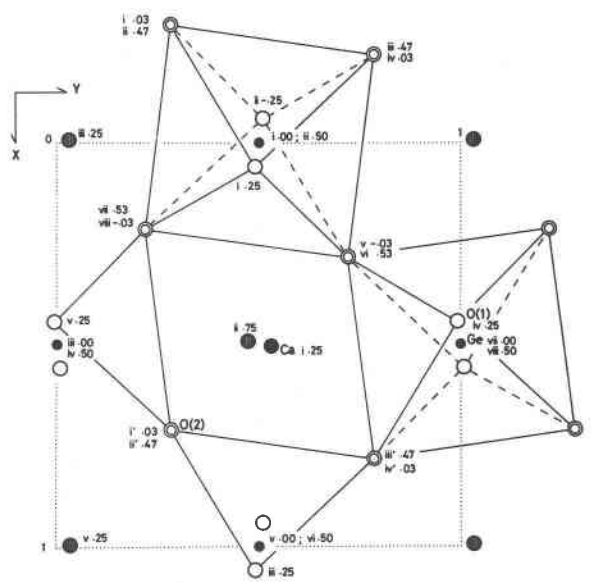

Fig. 2. Structure of $CaGeO_3$ perovskite projected on (001); Ca sites ruled, Ge sites solid, O(1) sites open, O(2) sites doubled. Each of the atoms is numbered with lower-case Roman numerals. Most atoms for which $0.5 < z < 1.0$ have been omitted for clarity.

[1]To receive a copy of structure factor tables and Table 5, order document AM-83-233 from the Business Office, Mineralogical Society of America, 2000 Florida Ave. NW, Washington, D. C. 20009. Please remit $1.00 in advance for microfiche.

Table 6. Comparison of tolerance factors and some structural characteristics such as B–O(1)–A and O(2)–O(2)–O(2) angles and bond-length distortions among orthorhombic $GdFeO_2$-type perovskites, ABO_3, based on single-crystal X-ray structure refinements.

	<B – O> (Å)	<A – O> (Å)	t_{obs}	Δ_B	Δ_A	B–O(1)–A i–i–i (°)	O(2)–O(2)–O(2) i–viii–i′ (°)	O(2)–O(2)–O(2) i′–ii′–vii (°)	t_{IR}	Reference
$SeMgO_3$	2.150	2.808	0.924	0.374	58.49	112.41	119.52	114.88	0.883	1
$ScAlO_3$	1.901	2.607	0.970	0.034	37.50	105.07(5)	133.60(4)	109.13(4)	0.830	2
$YAlO_3$	1.911	2.655	0.982	0.017	20.34	102.55(31)	145.89(68)	103.86(53)	0.884	3
$SmAlO_3$	1.899	2.657	0.989	0.001	8.66	100.18(13)	155.41(21)	100.66(16)	0.906	4
$MgSiO_3$*	1.790	2.476	0.978	0.226	27.31	103.8(15)	139.9(16)	107.7(15)	0.900	5
$MgSiO_3$*	1.791	2.474	0.977	0.002	28.27	103.3(13)	138.1(16)	108.2(16)	0.900	6
$CaTiO_3$	1.926	2.712	0.996	0.001	5.62	95.6	161.3	98.4	0.889	7
$YTiO_3$	2.039	2.800	0.971	0.177	37.69	105.67(15)	134.65(18)	107.82(15)	0.826	8
$LaTiO_3$	2.018	2.816	0.987	0.003	11.69	100.97(74)	151.62(57)	101.62(47)	0.874	8
$NdTiO_3$	2.022	2.803	0.980	0.025	21.73	103.47(12)	143.72(14)	104.49(12)	0.857	8
$SmTiO_3$	2.038	2.814	0.976	0.074	28.36	104.62(20)	139.65(24)	106.17(20)	0.847	8
$GdTiO_3$	2.039	2.811	0.975	0.170	32.48	105.04(12)	137.52(14)	106.66(12)	0.838	8
$InCrO_3$	1.987	2.708	0.964	0.096	38.40	105.18(16)	131.96(22)	110.39(19)	0.814	9
$SeMnO_3$	2.235	2.894	0.916	0.424	64.51	112.76	117.16	115.86		1
$LaMnO_3$#	2.018	2.818	0.987	3.75	16.44	101.15(16)	143.79(31)	101.89(26)	0.952	10
$PrMnO_3$#	2.037	2.823	0.980	5.55	27.51	100.91(16)	133.45(29)	103.61(26)	0.871	11
$YFeO_3$	2.015	2.771	0.972	0.081	34.26	104.67(29)	135.32(33)	108.09(31)	0.836	12
$PrFeO_3$	2.008	2.791	0.983	0.008	17.67	102.25(11)	146.48(17)	103.75(13)	0.873	13
$NdFeO_3$	2.011	2.790	0.981	0.007	20.24	102.89(11)	144.71(14)	104.53(12)	0.868	13
$SmFeO_3$	2.013	2.785	0.978	0.040	24.83	103.48(9)	141.46(11)	105.54(9)	0.857	13
$EuFeO_3$	2.013	2.783	0.978	0.038	26.85	103.64(11)	140.56(14)	105.82(12)	0.853	13
$GdFeO_3$	2.012	2.781	0.977	0.032	28.13	103.87(16)	140.19(15)	105.83(13)	0.848	13
$TbFeO_3$	2.012	2.775	0.975	0.047	30.17	104.03(9)	138.42(11)	106.79(9)	0.844	13
$DyFeO_3$	2.012	2.773	0.975	0.059	32.02	104.15(12)	137.22(14)	107.10(12)	0.839	13
$HoFeO_3$	2.010	2.768	0.974	0.054	33.36	104.36(13)	136.55(17)	107.44(14)	0.835	13
$ErFeO_3$	2.011	2.765	0.972	0.038	34.85	104.83(12)	135.72(14)	107.83(12)	0.831	13
$TmFeO_3$	2.011	2.763	0.972	0.029	35.87	104.67(13)	135.07(17)	108.26(15)	0.828	13
$YbFeO_3$	2.011	2.759	0.970	0.029	37.61	104.69(17)	134.00(20)	108.61(16)	0.825	13
$LuFeO_3$	2.010	2.755	0.969	0.030	38.62	105.01(15)	133.01(18)	109.30(15)	0.822	13
$SeCoO_3$	2.148	2.805	0.923	0.688	58.30	112.39	121.00	114.15		1
$TeCoO_3$	2.159	2.855	0.935	1.88	50.24	112.28	128.87	109.48		1
$SeNiO_3$	2.113	2.768	0.926	0.285	55.72	111.74	121.59	113.64		1
$SeCuO_3$	2.177	2.839	0.922	13.5	60.26	113.12	130.81	111.54		1
$SeZnO_3$	2.160	2.815	0.922	0.775	59.14	111.99	120.63	114.51		1
$CaGeO_3$	1.892	2.647	0.989	0.005	9.40	99.57(14)	154.72(18)	100.18(14)	0.923	14
$SrZrO_3$#	2.091	2.919	0.987	0.006	10.65	101.18(31)?	152.92(35)	101.12(27)	0.887	15
$BaCeO_3$#	2.241	3.128	0.987	0.044	10.57	101.13(62)	151.10(77)	102.97(76)	0.878	16
$BaPrO_3$#	2.223	3.111	0.990	0.001	9.63	100.99(97)	154.6(12)	101.8(10)	0.886	16
$NaTaO_3$#	1.978	2.765	0.988	0.001	8.23	99.51(6)	155.81(8)	99.43(6)	0.894	17

<B – O>: Mean atomic distances for B site (VI coordinate).
<A – O>: Mean atomic distances for A site (XII coordinate).
t_{obs} : Observed tolerance factor: $t=\langle A\text{–}O\rangle/\sqrt{2}\langle B\text{–}O\rangle$.
t_{IR} : Tolerance factor calculated from the Shannon & Prewitt's ionic radii (VI and XII coordinates for B and A site, respectively).
Δ_B : Bond-length distortion for B-site (VI coordinate).
Δ_A : Bond-length distortion for A-site (XII coordinate).
* : X-ray powder diffraction study.
\# : Neutron powder diffraction study.

References

(1) Kohn, Inoue, Horie, and Akimoto (1976).
(2) Sinclair, Eggleton, and Ringwood (1979).
(3) Diehl and Brandt (1975).
(4) Marezio, Dernier, and Remeika (1972).
(5) Yagi, Mao, and Bell (1978).
(6) Ito and Matsui (1978).
(7) Kay and Bailey (1957).
(8) MacLean, Ng, and Greedan (1979).
(9) Prewitt, C.T.: unpublished data.
(10) Elemans, Van Laar, Van Der Veen, and Loopstra (1971).
(11) Pollert and Jirak (1980).
(12) Coppens and Eibschutz (1965).
(13) Marezio, Remeika, and Dernier (1970).
(14) This study.
(15) Ahtee, Ahtee, Glazer, and Hewat (1976).
(16) Jacobson, Tofield, and Fender (1972).
(17) Ahtee and Darlington (1980).

The calculated powder diffraction pattern of $CaGeO_3$ perovskite for Cu$K\alpha$ radiation (λ = 1.5418Å) is given in Table 5[1]. This pattern shows that a $GdFeO_3$-type perovskite with a small unit cell distortion, such as that for $CaGeO_3$, is difficult to distinguish from a cubic one using only X-ray powder data. Because all of the strong reflections in this pattern can be indexed on a pseudocubic cell, it is easy to understand why Ringwood and Major (1967) and Prewitt and Sleight (1969) reported the symmetry of $CaGeO_3$ to be cubic.

Tilting of polyhedra in $GdFeO_3$-type perovskites (Pbnm)

Glazer (1972; 1975) proposed a classification of perovskites based on tilting of octahedra and has suggested that the overall symmetry follows that of the tilts in spite of displacements and distortions. Although the tilting of the octahedra has been shown to have a large effect on lattice parameters, the description has been difficult because of different factors involved: for example, although $SmAlO_3$ and $CaTiO_3$ have similar tilting angles of octahedra, the ratios of cell constants are very different between these crystals: a/b = 5.291/5.290 (= 1.0) and $c/\sqrt{2}$ = 5.285Å for $SmAlO_3$; a/b = 5.367/5.444 and $c/\sqrt{2}$ = 5.405Å for $CaTiO_3$. The following factor, newly defined here, makes it possible to describe the tiltings and/or distortions in a systematic way: we define the *observed tolerance factor*

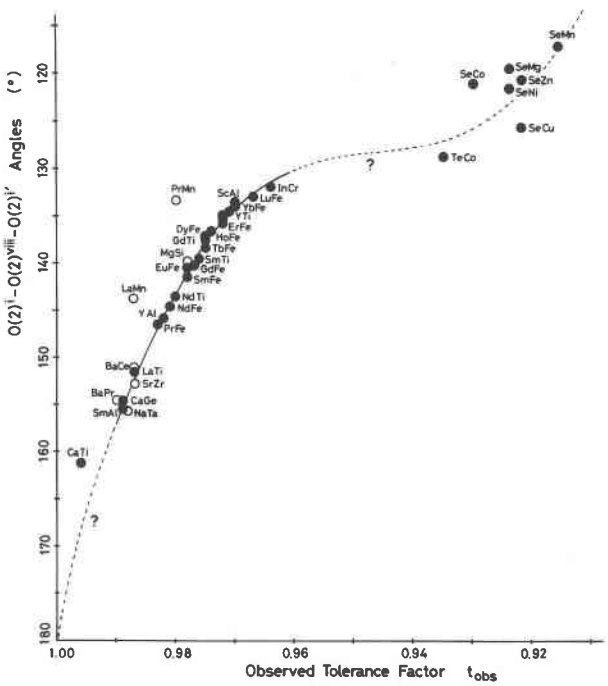

Fig. 3. $O(2)^{i}$–$O(2)^{viii}$–$O(2)^{i\prime}$ angle *vs.* t_{obs} for the $GdFeO_3$-type perovskites. Solid circles represnt single-crystal X-ray results; open circles X-ray or neutron powder; shaded circle X-ray film with single crystal. The line is based on a polynomial equation (C Fit) shown in Table 7.

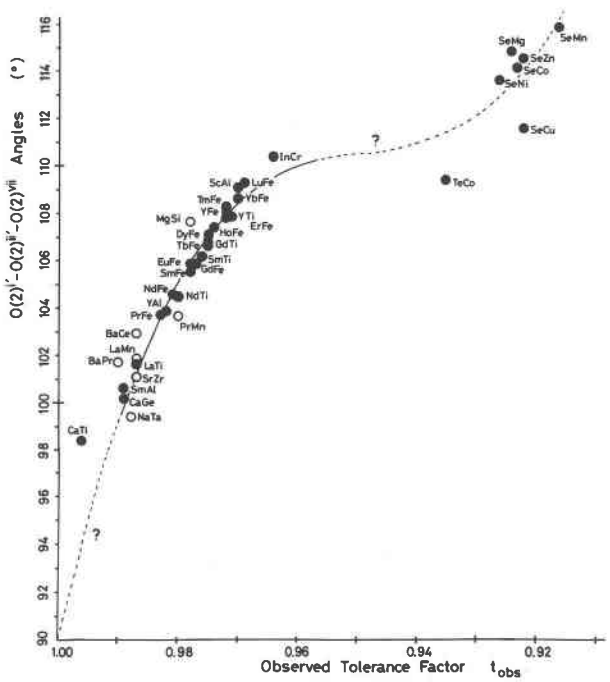

Fig. 4. $O(2)^{i\prime}$–$O(2)^{ii\prime}$–$O(2)^{vii}$ angle *vs.* t_{obs} for the $GdFeO_3$-type perovskites. Samples plotted are the same as those in Fig. 3. The line is based on a polynomial equation (C Fit) shown in Table 7.

based on the atomic parameters obtained from X-ray or neutron studies as follows:

$$t_{obs} = \langle A\text{–}O\rangle/\sqrt{2}\langle B\text{–}O\rangle,$$

where $\langle$A–O$\rangle$ and $\langle$B–O$\rangle$ are the mean interatomic distances with twelve and six coordination for A and B sites, respectively. The coordination numbers are fixed for all $GdFeO_3$-type perovskites in order to maintain the same basis for comparison of structures with different coordinations. The t_{obs} values calculated from the atomic parameters are listed in Table 6.

The variations of angles of $O(2A)^{i}$–$O(2)^{viii}$–$O(2)^{i\prime}$ [xy], $O(2)^{i\prime}$–$O(2)^{ii\prime}$–$O(2)^{vii}$ [yz], and B^{i}–$O(1)^{i}$–A^{i} are shown in Figures 3, 4, and 5 as functions of t_{obs}. Some distinct features are evident among the $GdFeO_3$-type perovskites: (1) The angles and bond length distortions concentrate clearly within two distinct groups t_{obs} = 0.96–0.99 (group I) and 0.93–0.92 (group II, including selenides and tellurides) with a data gap in t_{obs} between the two groups. $CaGeO_3$ and $SmAlO_3$ are characterized as less-distorted perovskites (t_{obs} = 0.989) and there is also a data gap between them and cubic perovskites (t_{obs} = 1.00), except for $CaTiO_3$. (2) There are systematic relationships between the angles showing the tilting of polyhedra and t_{obs}: (a) as t_{obs} decreases, the angle $O(2)^{i}$–$O(2)^{viii}$–$O(2)^{i\prime}$ decreases (see Fig. 3); (b) as the t_{obs} decreases, the $O(2)^{i\prime}$–$O(2)^{ii\prime}$–$O(2)^{vii}$ angle and the B^{i}–$O(1)^{i}$–A^{i} bond angle increase (see Fig. 4 and 5). (3) Table 7 shows that, in group I, the tilting of polyhedra versus t_{obs} can be interpolated

using the polynominal approximation of $y = \Sigma a_j\{(1\text{-}t_{obs})^j \times 10^3\}$ (j = 0,1,2,..,n; where n = 2 or 3) (see "A Fit" in this table). (4) Also, these curves can be extended to fit over the full range as shown in "C Fit" of Table 7.

The distortions of polyhedra in $GdFeO_3$-type perovskites

It is useful to plot distortions of polyhedra as well as tilts versus t_{obs}. Figures 6 and 7 show the correlation of bond-length distortions Δ_A and Δ_B versus t_{obs} for the A and B sites, respectively. Figure 6 shows that bond-length distortions for the larger A site have a systematic relationship with t_{obs}: (1) As the value of t_{obs} decreases, the distortions increase. (2) The trend can be approximated as a linear function within each of the groups, I and II. (3) The equations for distortions versus t_{obs} allow an interpolation within a group but does not permit an extrapolation. (4) The fit of the polynomial approximation, shown by the form of $R_k = \Sigma\{|\,|Y(obs)|-|Y(calc)|\,|/|Y(obs)|\}_k$, is not as good for distortions of polyhedra as it is for tilting (see Table 7). Although a comparison of bond-length distortion for the B site indicates similar characteristics to that of Δ_A, there is no strong systematic relationship (Fig. 7).

Application for germanates and silicates

The systematic relationships observed in Figures 3 to 7 suggest that it might be possible to predict the deformation of perovskites containing various ions. For this purpose, we must be able to estimate the value of t_{obs} from known quantities such as ionic radii. In Figure 8, we

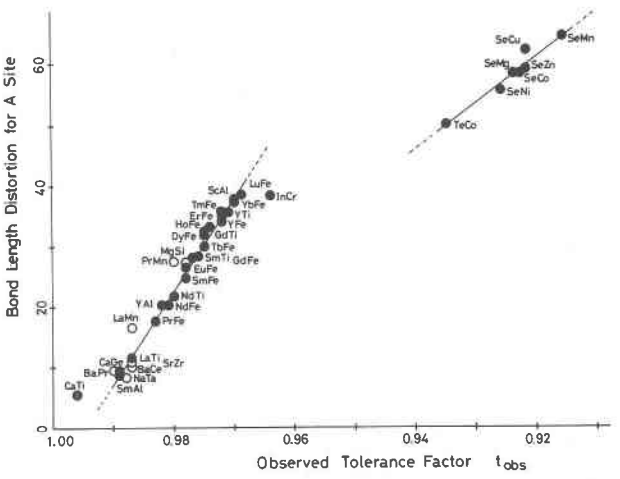

Fig. 6. Bond-length distortion for A site *vs.* t_{obs} for the $GdFeO_3$-type perovskites. Samples plotted are the same as those in Fig. 3.

plot the Goldschmidt tolerance factor, $t_{IR} = (r_A + r_O)/\sqrt{2}(r_B + r_O)$ versus t_{obs} for the perovskite crystals shown in Table 6, where r_A, r_B and r_O (= 1.4 Å) are the empirical ionic radii of the respective ions in the compound ABO_3 (Shannon and Prewitt, 1969; Shannon, 1976). Radii data for coordination numbers eight (A site) and six (B site) were used because values for twelve coordination for

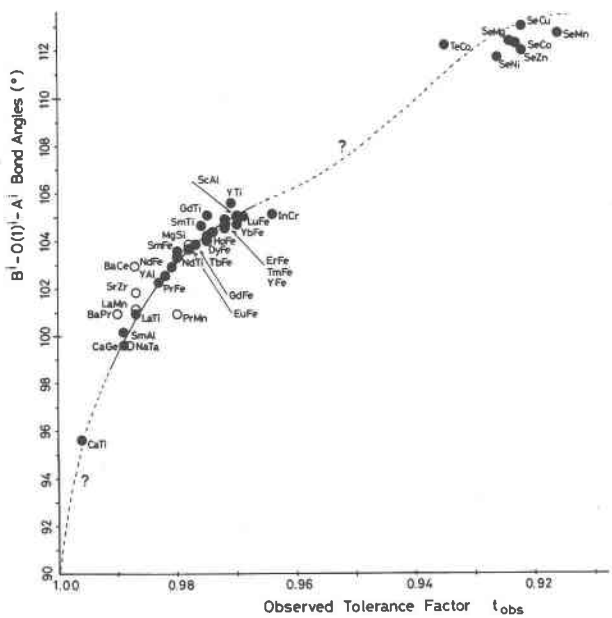

Fig. 5. B^i–O(1)^i–A^i angle *vs.* t_{obs} for the $GdFeO_3$-type perovskite. Samples plotted are the same as those in Fig. 3. The line is based on a polynomial equation (C Fit) shown in Table 7.

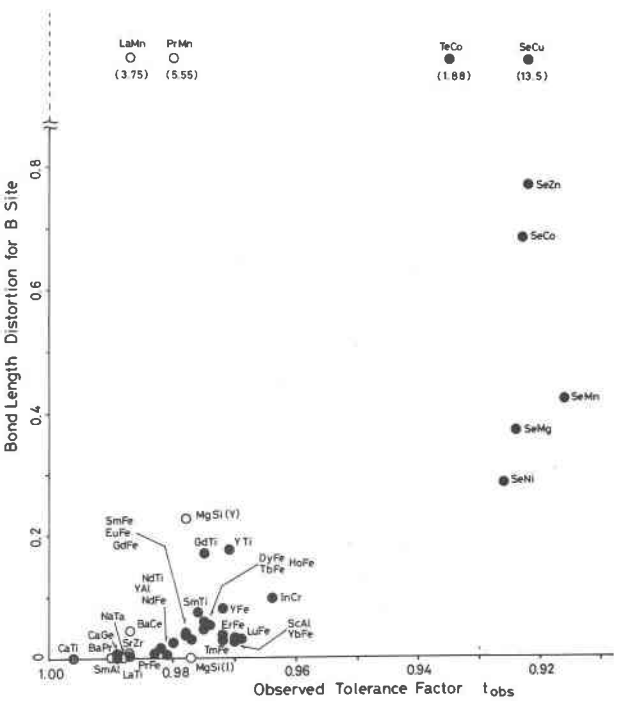

Fig. 7. Bond-length distortion for B site *vs.* t_{obs} for the $GdFeO_3$-type perovskites. Samples plotted are the same as those in Fig. 3. For $MgSiO_3$, Y and I represent values after Yagi *et al.* (1978) and Ito and Matsui (1978), respectively.

Table 7. The polynominal equations relating some bond angles and bond-length distortion versus t_{obs} using the mean squares method with least-squares calculations. The form is given by: $Y = \Sigma\, a_j\{(1\text{-}t_{obs}) \times 10^3\}^j$ (j = 0,1,2,...,n, where n = 3, 4, or 5).

	a_0	a_1	a_2	a_3	a_4	R_k	Reference
A Fit (Group I) ($0.96 < t_{obs} \leq 0.99$)							
$O(2)^i$–$O(2)^{viii}$–$O(2)^{i'}$	167.353	−0.88694	−0.031787	0.80562×10^{-3}		0.009	Fig. 3
$O(2)^{i'}$–$O(2)^{ii'}$–$O(2)^{vii}$	94.153	0.62812	−0.004793			0.002	Fig. 4
B^i–$O(1)^i$–A^i	93.703	0.67376	−0.009870			0.002	Fig. 5
Δ_A	15.340	−2.41560	0.206090	-0.33625×10^{-2}		0.024	Fig. 6
B Fit (Group I + Cubic) ($0.96 < t_{obs} \leq 1.00$)							
$O(2)^i$–$O(2)^{viii}$–$O(2)^{i'}$	180.001	−3.44519	0.149365	-0.45824×10^{-2}	0.57285×10^{-4}	0.008	Fig. 3
$O(2)^{i'}$–$O(2)^{ii'}$–$O(2)^{vii}$	89.998	1.50629	−0.069647	0.20036×10^{-2}	-0.22033×10^{-4}	0.002	Fig. 4
B^i–$O(1)^i$–A^i	90.019	1.20693	−0.033576	0.33067×10^{-3}		0.002	Fig. 5
Δ_A	−0.0015	0.68943	−0.013916	0.31847×10^{-2}	-0.69645×10^{-4}	0.023	Fig. 6
C Fit (Groups I and II + Cubic) ($0.91 < t_{obs} \leq 1.00$)							
$O(2)^i$–$O(2)^{viii}$–$O(2)^{i'}$	179.956	−2.70904	0.048539	-0.29879×10^{-3}		0.025	Fig. 3
$O(2)^{i'}$–$O(2)^{ii'}$–$O(2)^{vii}$	90.018	1.12058	−0.020962	0.13474×10^{-3}		0.004	Fig. 4
B^i–$O(1)^i$–A^i	90.034	1.25746	−0.040800	0.61616×10^{-3}	-0.32303×10^{-5}	0.003	Fig. 5
Δ_A	−0.2526	0.37869	0.066647	-0.15607×10^{-2}	0.98440×10^{-5}	0.036	Fig. 6

t_{obs}: The observed tolerance factor
$R_k = \Sigma\,\{||Y(obs)|-|Y(calc)||/|Y(obs)|\}$; For the calculation of $O(2)^i$–$O(2)^{viii}$–$O(2)^{i'}$, Y=180−Y.

many ions are lacking. It is very significant that the $GdFeO_3$-type perovskites with the same B ion can be characterized as a linear function in the t_{IR}–t_{obs} diagram, and that each function for the different B ions has almost the same slope. These characteristics make the estimation of t_{obs} possible for structures containing arbitrary kinds of ions.

Let us consider several germanates and silicates because of their geophysical importance. Average gradients of the t_{obs}–t_{IR} lines of titanates, aluminates, and orthoferrites were assumed for germanates and silicates making use of the data for $CaGeO_3$ (this study) and $MgSiO_3$ (Yagi *et al.*, 1978). The estimated values of t_{obs}, which we shall call t'_{obs}, can be derived from the assumption that:

$$t'_{obs} = 0.274\, t_{IR} + 0.736 \quad (1)$$

for germanates, and

$$t'_{obs} = 0.274\, t_{IR} + 0.731 \quad (2)$$

for silicates (see Fig. 8).

$SrGeO_3$ is known to crystallize as a cubic perovskite (Shimizu *et al.*, 1970). The t'_{obs} value of 1.003 ($SrGeO_3$) estimated from t_{IR} = 0.975 is consistent with the observation that $SrGeO_3$ is a cubic perovskite. The value of t'_{obs} = 1.019 for hexagonal $BaGeO_3$ (Shimizu *et al.*, 1970) may show that the orthorhombic $GdFeO_3$-type perovskites can be separated crystallographically from hexagonal ones. On the other hand, for the silicate $CaSiO_3$, which was reported to transform into a cubic perovskite at P = 160 kbar and T = 25°C (Liu and Ringwood, 1975), the value of t'_{obs} = 1.002 (t_{IR} = 0.99) is close to 1.0, in accord with the formation of cubic perovskite.

A cubic $CdGeO_3$ perovskite with a = 3.7Å has been reported to exist at 130 kbar and 900°C (Ringwood and Major, 1967). The value of t'_{obs} = 0.987 (t_{IR} = 0.916), determined from Equation (1), is close to those of $CaGeO_3$ and $SmAlO_3$. This means that $CdGeO_3$ should crystallize in space group *Pbnm*, but with more distorted polyhedra than is found for $CaGeO_3$. Because $CaGeO_3$ was previously reported incorrectly as cubic perovskite, a more detailed study of the symmetry for $CdGeO_3$ is required. If $CdGeO_3$ is orthorhombic, the t'_{obs} value predicts a crystal structure similar to that of $LaTiO_3$: $O(2)^i$–$O(2)^{viii}$–$O(2)^{i'}$ = 152°, $O(2)^{i'}$–$O(2)^{ii'}$–$O(2)^{vii}$ = 102°, Ge^i–$O(1)^i$–Cd^i = 101°, and $\Delta_{A(=Cd)}$ = 11. $MnGeO_3$ quenched from 250 kbar and 1400–1800°C has been found to be orthorhombic (Liu, 1976b). The value of t'_{obs} = 0.973 (t_{IR} = 0.865) supports this report and predicts the space group *Pbnm* (or $Pbn2_1$). Liu (1977) reported $MgGeO_3$ as an orthorhombic perovskite, having space group *Pmmm* or *P*222. Examination of the t_{obs}–t_{IR} diagram shows that $MgGeO_3$ is within the stability of the $GdFeO_3$-type perovskite (t'_{obs} = 0.966; t_{IR} = 0.839) and has similar characteristics to $InCrO_3$. However, because the report for $MgGeO_3$ was based on powder data of five mixed phases, it is also recommended that the space group be reexamined.

It should be emphasized that the data are consistent with $MgSiO_3$ (Yagi *et al.*, 1978; Ito and Matsui, 1978) being a $GdFeO_3$-type perovskite (see Figs. 3 to 7). In contrast, Madon, Bell, Mao, and Poirier (1980) assigned tetragonal symmetry to $MgSiO_3$ ($a = b$ = 9.3, c = 13.1Å), based on lattice parameters measured using electron diffraction patterns. Their observations, however, are not sufficient to confirm the symmetry and their conclusion may result from other factors such as twinning or pseudosymmetry. It should be noted that an experiment using

only electron microscopy is not sufficient to determine the symmetry.

We may use the observed relationship to predict values of t'_{obs} for perovskites of some germanate and silicate compounds which have not yet been synthesized. For this purpose, the values of t'_{obs} associated with various cations were calculated for germanates and silicates from t_{IR} and are shown in Table 8. The compounds for which the t'_{obs} lies within the range for group I would probably crystallize as orthorhombic perovskites and have the tilting and distortion of oxygen polyhedra as estimated from Table 7: these are $FeGeO_3$ (t'_{obs} = 0.969), $CoGeO_3$ (0.967), and $ZnGeO_3$ (0.967) for germanates, and $MnSiO_3$ (t'_{obs} = 0.985), $FeSiO_3$ (0.981), $CoSiO_3$ (0.979), and $ZnSiO_3$ (0.978) for silicates. On the other hand, $BaSiO_3$ (t'_{obs} = 1.035) and $SrSiO_3$ (1.017) should not occur as the $GdFeO_3$-type perovskite. However, the above discussion illustrates only one geometrical aspect concerning crystallization of orthorhombic perovskites; often other factors such as crystal-field effects determine what phases are stable. For example, although $FeSiO_3$ is one of the possible orthorhombic perovskites (see Table 8), it is thought to be unstable with respect to mixed oxides (Yagi *et al.*, 1978).

Table 8. Estimated values of t_{obs} for some germanates and silicates.

	t_{IR}	t'_{obs}		t_{IR}	t'_{obs}
Germanates			Silicates		
$MgGeO_3$	0.839	0.966			
			$CaSiO_3$	0.990	1.002
$MnGeO_3$	0.865	0.973	$MnSiO_3$	0.927	0.985
$FeGeO_3$	0.850	0.969	$FeSiO_3$	0.911	0.981
$CoGeO_3$	0.843	0.967	$CoSiO_3$	0.904	0.979
$ZnGeO_3$	0.843	0.967	$ZnSiO_3$	0.904	0.979
$SrGeO_3$	0.975	1.003	$SrSiO_3$	1.045	1.017
$CdGeO_3$	0.916	0.987	$CdSiO_3$	0.982	0.986
$BaGeO_3$	1.033	1.019	$BaSiO_3$	1.108	1.035

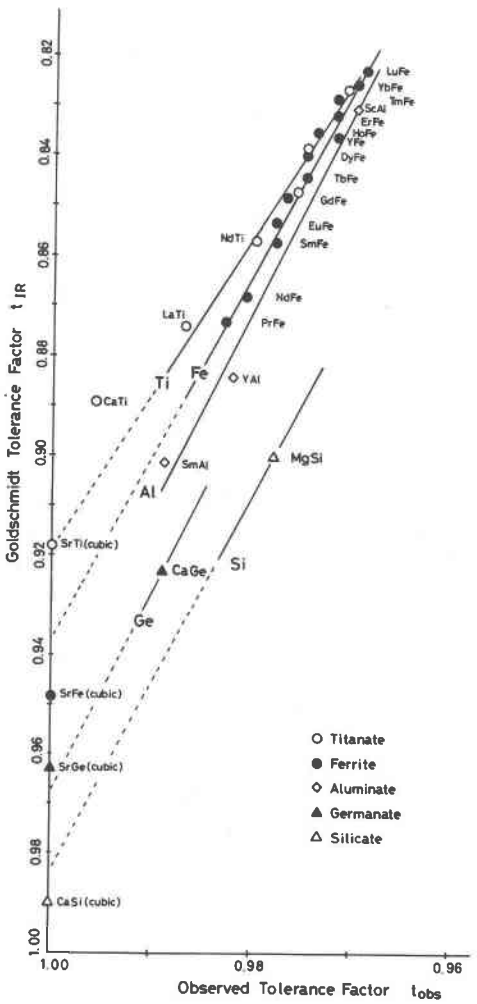

Fig. 8. The t_{obs}–t_{IR} diagram of some $GdFeO_3$-type perovskites such as orthoferrites, titanates, aluminates, germanate, and silicates.

Summary

$CaGeO_3$ perovskite is orthorhombic *(Pbnm)* and isostructural with $GdFeO_3$. The oxygen polyhedra are less tilted and less distorted than those of most $GdFeO_3$-type perovskites. Comparison between structural characteristics and t_{obs} has made possible useful predictions for the existence of previously-unknown $GdFeO_3$-type perovskites. The following predictions are obtained for germanate and silicates: (1) $CdGeO_3$ should crystallize as an orthorhombic perovskite rather than a cubic one; (2) the perovskite form of $MgSiO_3$ probably has the $GdFeO_3$-type structure; (3) the space group, *Pmmm* (or *P*222), reported for a $MgGeO_3$ perovskite should be reexamined with the possibility of it being *Pbnm;* (4) in the geometrical view of crystals, germanate and silicate perovskites containing Mg, Mn, Co, Fe, and Zn ions in the large A site should have the $GdFeO_3$-type structure.

Acknowledgments

The authors would like to thank Dr. R. Jeanloz for suggestions that we reexamine the symmetry of $CaGeO_3$, Dr. J. Bass for valuable discussions, and Prof. P. Coppens for providing the original least-squares program of RADIEL. Computations were carried out on the UNIVAC 1110 at the Computer Center of SUNY at Stony Brook. This project has been supported by NSF grants EAR 81-20950 and EAR 80-18343.

References

Ahtee, A., Ahtee, M., Glazer, A. M. and Hewat, A. W. (1976) The structure of orthorhombic $SrZrO_3$ by neutron powder diffraction. Acta Crystallographica, B32, 3243–3246.

Ahtee, M. and Darlington, C. N. W. (1980) Structures of $NaTaO_3$ by neutron powder diffraction. Acta Crystallographica, B36, 1007–1014.

Batsanov, S. S. (1968) The concept of electronegativity. Conclusion and prospects. Russian Chemical Reviews, 37, 332–351.

Becker, P. J. and Coppens, P. (1974) Extinction within the limit of validity of the Darwin transfer equations. I. General formal-

isms for primary and secondary extinction and their application to spherical crystals. Acta Crystallographica, A30, 129–147.

Coppens, P. and Eibschutz, M. (1965) Determination of the crystal structure of yttrium orthoferrite and refinement of gadolinium orthoferrite. Acta Crystallographica, 19, 524–531.

Coppens, P., Guru Row, T. N., Leung, P., Stevens, E. D., Becker, P. J. and Yang, Y. W. (1979) Net atomic charges and molecular dipole moments from spherical-atom X-ray refinements, and the relation between atomic charge and shape. Acta Crystallographica, A35, 63–72.

Diehl, R. and Brandt, G. (1975) Crystal structure refinement of $YAlO_3$, a promising laser material. Material Research Bulletin, 10, 85–90.

Elemans, J. B. A. A., Van Laar, B., Van Der Veen, K. R. and Loopstra, B. O. (1971) The crystallographic and magnetic structures of $La_{1-x}Ba_xMn_{1-x}Me_xO_3$ (Me = Mn or Ti). Journal of Solid State Chemistry, 3, 238–242.

Fukamachi, T. (1971) Mean X-ray scattering factors calculated from analytical Roothaan–Hartree–Fock wave functions by Clementi. Technical Report of the Institute of Solid State Physics, University of Tokyo, B12.

Glazer, A. M. (1972) The classification of tilted octahedra in perovskite. Acta Crystallographica, B28, 3384–3392.

Glazer, A. M. (1975) Simple ways of determining perovskite structures. Acta Crystallographica, A31, 756–762.

Ibers, J. A. and Hamilton, W. C. (Eds.) (1974) International Tables for X-Ray Crystallography, vol. IV. Birmingham, Kynoch Press.

Ito, E. and Matsui, Y. (1978) Synthesis and crystal-chemical characterization of $MgSiO_3$ perovskite. Earth and Planetary Science Letters, 38, 443–450.

Jacobson, A. J., Tofield, B. C. and Fender, B. E. F. (1972) The structures of $BaCeO_3$, $BaPrO_3$ and $BaTbO_3$ by neutron diffraction: Lattice parameter relations and ionic radii in O-perovskites. Acta Crystallographica, B28, 956–961.

Kay, H. F. and Bailey, P. C. (1957) Structure and properties of $CaTiO_3$. Acta Crystallographica, 10, 219–226.

Kohn, K., Inoue, K., Horie, O. and Akimoto, S. (1976) Crystal Chemistry of $MSeO_3$ and $MTeO_3$ (M = Mg, Mn, Co, Ni, Cu and Zn). Journal of Solid State Chemistry, 18, 27–37.

Liebermann, R. C., Jones, L. E. A. and Ringwood, A. E. (1977) Elasticity of aluminate, titanate, stannate and germanate compounds with the perovskite structure. Physics of the Earth and Planetary Interiors, 14, 165–178.

Liu, L. (1976a) Orthorhombic perovskite phases observed in olivine, pyroxene and garnet at high pressures and temperatures. Physics of the Earth and Planetary Interiors, 11, 289–298.

Liu, L. (1976b) High-pressure phases of Co_2GeO_4, Ni_2GeO_4, Mn_2GeO_4 and $MnGeO_3$: Implications for the germanate–silicate modeling scheme and the earth's mantle. Earth and Planetary Science Letters, 31, 393–396.

Liu, L. (1977) Post-ilmenite phases of silicates and germanates. Earth and Planetary Science Letters, 35, 161–168.

Liu, L. and Ringwood, A. E. (1975) Synthesis of a perovskite-type polymorph of $CaSiO_3$. Earth and Planetary Science Letters, 28, 209–211.

MacLean, D. A., Ng, H. and Greedan, J. E. (1979) Crystal structures and crystal chemistry of the $RETiO_3$ perovskites: RE = La, Nd, Sm, Gd, Y. Journal of Solid State Chemistry, 30, 35–44.

Madon, M., Bell, P. M., Mao, H. K. and Poirier, J. P. (1980) Transmission electron diffraction and microscopy of synthetic high pressure $MgSiO_3$ phase with perovskite structure. Geophysical Research Letters, 7, 629–632.

Marezio, M., Dernier, P. D. and Remeika, J. P. (1972) The crystal structures of orthorhombic $SmAlO_3$ and of trigonal $NdAlO_3$. Journal of Solid State Chemistry, 4, 11–19.

Marezio, M., Remeika, J. P. and Dernier, P. D. (1970) The crystal chemistry of the rare earth orthoferrites. Acta Crystallographica, B26, 2008–2022.

Pollert, E. and Jirak, Z. (1980) Study of $Pr_{1-x}Mn_{1+x}O_3$ perovskite. Journal of Solid State Chemistry, 35, 262–266.

Prewitt, C. T. and Sleight, A. W. (1969) Garnet-like structures of high-pressure cadmium germanate and calcium germanate. Science, 163, 386–387.

Reid, A. F. and Ringwood, A. E. (1975) High-pressure modification of $ScAlO_3$ and some geophysical implications. Journal of Geophysical Research, 80, 3363–3370.

Ringwood, A. E. and Major, A. (1967) Some high-pressure transformations of geophysical significance. Earth and Planetary Science Letters, 2, 106–110.

Ringwood, A. E. and Seabrook, M. (1963) High-pressure phase transformations in germanate pyroxenes and related compounds. Journal of Geophysical Research, 68, 4601–4609.

Sasaki, S., Prewitt, C. T. and Liebermann, R. C. (1981) Single-crystal X-ray study of a $CaGeO_3$ perovskite. (abstr.) IUCr XIIth Congress in Ottawa, Canada. Acta Crystallographica A37, C-165.

Shannon, R. D. (1967) Revised effective ionic radii and systematic studies of interatomic distances in halides and chalcogenides. Acta Crystallographica, A32, 751–767.

Shannon, R. D. and Prewitt, C. T. (1969) Effective ionic radii in oxides and fluorides. Acta Crystallographica, B25, 925–946.

Shimizu, Y., Syono, Y. and Akimoto, S. (1970) High-pressure transformations in $SrGeO_3$, $SrSiO_3$, $BaGeO_3$ and $BaSiO_3$. High Temperatures–High Pressures, 2, 113–120.

Sinclair, W., Eggleton, R. A. and Ringwood, A. E. (1979) Crystal synthesis and structure refinement of high-pressure $ScAlO_3$ perovskite. Zeitschrift für Kristallographie, 149, 307–314.

Tokonami, M. (1965) Atomic scattering factor for O^{2-}. Acta Crystallographica, 19, 486.

Wuensch, B. J. and Prewitt, C. T. (1965) Corrections for X-ray absorption by a crystal of arbitrary shape. Zeitschrift für Kristallographie, 122, 24–59.

Yagi, T., Mao, H. and Bell, P. M. (1978) Structure and crystal chemistry of perovskite-type $MgSiO_3$. Physics and Chemistry of Minerals, 3, 97–110.

Zachariasen, W. H. (1967) A general theory of X-ray diffraction in crystals. Acta Crystallographica, 23, 558–564.

Manuscript received, August 11, 1982;
accepted for publication, March 21, 1983.